# Infrared spectroscopic study of CuO: Signatures of strong spin-phonon interaction and structural distortion

A. B. Kuz'menko,[1] D. van der Marel,[2] P. J. M. van Bentum,[3] E. A. Tishchenko,[1] C. Presura,[2] and A. A. Bush[4]
[1]*P. L. Kapitza Institute for Physical Problems RAS, Kosygina street, 2, Moscow, 117334, Russia*
[2]*Solid State Physics Laboratory, University of Groningen, Nijenborgh 4, 9747 AG Groningen, The Netherlands*
[3]*High Field Magnet Laboratory, University of Nijmegen, 6525 ED, Nijmegen, The Netherlands*
[4]*Moscow State Institute of Radiotechnics, Electronics and Automation, Vernadskogo pr., 78, Moscow, 117464, Russia*
(Received 24 January 2000; revised manuscript received 26 June 2000; published 2 February 2001)

Optical properties of single-crystal monoclinic CuO in the range 70–6000 $cm^{-1}$ were studied at temperatures from 7 to 300 K. Normal reflection spectra were obtained from the (001) and (010) crystal faces thus giving separate data for the $A_u$ and $B_u$ phonon modes excited in the purely transverse way (TO modes). Mode parameters, including polarizations of the $B_u$ modes not determined by the crystal symmetry, were extracted by the dispersion analysis of reflectivity curves as a function of temperature. Spectra of all the components of the optical conductivity tensor were obtained using the Kramers-Kronig method recently extended to the case of the low-symmetry crystals. The number of strong phonon modes is in agreement with the factor-group analysis for the crystal structure currently accepted for the CuO. However, several ''extra'' modes of minor intensity are detected; some of them are observed in the whole studied temperature range, while existence of others becomes evident at low temperatures. Comparison of frequencies of ''extra'' modes with the available phonon dispersion curves points to possible ''diagonal'' doubling of the unit cell $\{\mathbf{a},\mathbf{b},\mathbf{c}\}\rightarrow\{\mathbf{a}+\mathbf{c},\mathbf{b},\mathbf{a}\text{-}\mathbf{c}\}$ and formation of the superlattice. The previously reported softening of the $A_u^3$ mode ($\sim$400 $cm^{-1}$) with cooling at $T_N$ is found to be $\sim$10% for the TO mode. The mode is very broad at high temperatures and strongly narrows in the antiferromagnetic phase. We attribute this effect to strong resonance coupling of this mode to optical or acoustic bimagnons and reconstruction of the magnetic excitations spectrum at the Néel point. A significant anisotropy of $\epsilon^{\infty}$ is observed: it was found to be 5.9 along the **b** axis, 6.2 along the [101] chains, and 7.8 along the $[10\overline{1}]$ chains. The transverse effective charge $e_T^*$ is more or less isotropic; its value is about two electrons.

DOI: 10.1103/PhysRevB.63.094303 PACS number(s): 78.20.Ci, 78.20.Bh, 78.30.−j, 71.27.+a

## I. INTRODUCTION

Since 1986 the interest of cupric oxide CuO has been mostly governed by its close relation to the problem of high-$T_c$ superconductivity. In addition to the role of the parent compound of all the high-$T_c$ materials with $CuO_2$ planes, it has a number of physical and chemical features common to several undoped antiferromagnetic (AFM) cuprates, (e.g., $La_2CuO_4$, $YBa_2Cu_3O_6$): similar copper coordination and electronic state, Cu-O distances, values of localized magnetic moments, superexchange constants, low-dimensionality of magnetism, etc.

CuO, however, is a quite interesting system in its own right. Although $Cu^{2+}$ ions are expected to be in the $3d^9$ state with one $3d$ hole per atom, this transition-metal (TM) oxide is a strongly correlated insulator of the ''charge-transfer'' type according to the theory of Zaanen, Sawatzky, and Allen;[1] the holes are well localized forming local magnetic moments. CuO undergoes a two-stage magnetic transition: at $T_{N1}=230$ K an incommensurate magnetic structure is observed, while at $T_{N2}=213$ K spins order parallel to the $b$ axis antiferromagnetically along the $[10\overline{1}]$ chains and ferromagnetically along the [101] chains.[2] From the analysis of the spin-wave velocity[2,3] it was found that the exchange constant along the $[10\overline{1}]$ chains (60–80 meV) is several times larger than this value along any other direction. The anomalous temperature dependence of the magnetic susceptibility[4] points to low-dimensional, or, at least, highly anisotropic character of magnetic interactions and persistency of spin correlations at temperatures well above the Néel point.[5,6]

Another feature of the cupric oxide is the low-symmetry monoclinic lattice, which distinguishes it from the other TM monoxides, e.g., MnO, FeO, CoO, and NiO with the rock-salt structure. It is a prominent manifestation of the Jahn-Teller effect: in the high-symmetry octahedral position characteristic to the cubic structure, the $Cu^{2+}$ ion would have degenerate $d_{x^2-y^2}$ and $d_{z^2}$ orbitals, which is energetically unfavorable, and therefore tends to displace away from the symmetry position. This tendency is so strong that CuO has not just a distorted cubic lattice, but a completely different monoclinic tenorite structure.

Several groups[7–13] have reported results of infrared (IR) spectroscopic studies of powder as well as single-crystal specimens of CuO. The interpretation of infrared spectra was always embarrassed by the low crystal symmetry, especially for the case of polycrystalline samples. Kliche and Popovic[10] have measured infrared spectra of sintered powder samples as a function of temperature and assigned strong IR-active modes to the species $A_u$ and $B_u$ by comparison of frequencies with those in PdO. They also reported an additional broad mode at about 414 $cm^{-1}$ the intensity of which increases drastically with cooling down below $T_N$ and suggested that it is a zone-boundary phonon mode which becomes IR active because of IR absorption from AFM superstructure. It is evident now that it was a manifestation of the anomalous softening of the $A_u^3$ mode reported by Homes *et al.*[13]

 

It has been a serious problem to obtain single crystals of CuO suitable for quantitative infrared studies. Guha *et al.*[11] have succeeded to measure infrared polarized spectra of single crystals of CuO at room temperature (RT) and account for low-symmetry effects in data analysis. They have measured reflectivity from the $(1\bar{1}0)$ natural face and modelled spectra by the dielectric function formulas adapted to monoclinic crystals.[14] However, due to inconvenient crystal orientation in their experiment mixed LO-TO modes were excited, the properties of which depend on the wave vector direction.

Homes *et al.*[13] presented single-crystal infrared spectra as a function of temperature. Again, however, only the $(1\bar{1}0)$ crystal surface was accessible for optical experiments, and mixed LO-TO modes were actually observed. An appreciable (about 5%) sharp softening of the $\sim 440$ cm$^{-1}$ Reststrahlen band for the $E \perp b$ upon cooling down was definitely registered at the Néel transition. Spectra were fitted with introduction of $3\,A_u$ and $3\,B_u$ phonon modes only. No new phonon structures at the magnetically ordered phase were reported indicating absence of a crystal superlattice below $T_{N2}$.

This statement sounds puzzling in a view of observation by Chen *et al.*[15] of five modes at low temperatures in the Raman spectra. Authors have assigned these modes to folded phonons; as a folding mechanism, a strong spin-phonon interaction was proposed. The most intense mode 240 cm$^{-1}$ hardens strongly with decreasing temperature, which was attributed[15] to an additional lattice rigidity due to magnetization.

There is a serious inconsistency concerning structure and parameters of IR-active phonon modes, especially at high frequencies. For instance, the deviations in resonance frequency of these modes reported by different groups are too significant to be explained by experimental errors, isotope effect, crystal nonstoiochiometry, etc. In our opinion, the explanation lies in the intermediate LO-TO nature of the observed modes and corresponding uncertainty of phonon parameters, especially for the high-frequency intense modes with large LO-TO splitting. Moreover, no infrared data so far were reported where the $A_u$ and $B_u$ modes were completely separated. Parameters of the $A_u$ modes were extracted at best from the single-crystal spectra for $E \perp c$ where the $B_u$ modes are also present.

In this paper we aimed to resolve this uncertainty by separate measurement of the characteristics of purely TO $A_u$ and $B_u$ modes. For monoclinic crystals the only option for observation of the $B_u$ TO modes is to measure normal reflectivity from the (010) face (the $ac$ plane). To study the $A_u$ TO modes any crystal plane containing the $b$ axis, e.g. (001) face, may suffice. We succeeded to obtain these crystal faces with a sufficiently large area, allowing to perform reliable measurements and quantitative analysis of the data as described below.

## II. CRYSTAL STRUCTURE AND FACTOR-GROUP ANALYSIS

Cupric oxide CuO, unlike other TM monoxides, crystallizes in a low-symmetry monoclinic tenorite structure (Fig. 1). It is generally accepted, following Åsbrink and Norrby,[16] that at room temperature the space group is $C_{2h}^6$ $(C2/c)$; there are four CuO molecules in the unit cell with dimensions $a=4.6837$ Å, $b=3.4226$ Å, $c=5.1288$ Å, $\beta=99.54°$, and two CuO units in the primitive cell; the copper and oxygen occupy the $C_i$ and $C_2$ symmetry positions correspondingly. Each copper atom is situated in the center of the oxygen parallelogram. Each oxygen atom, in turn, has a distorted tetrahedral copper coordination. The adjacent $CuO_4$ parallelograms form two sets of ribbons propagating along the $[110]$ and the $[1\bar{1}0]$ directions. The structure can be also considered as being composed from two types of zig-zag Cu-O chains running along the $[101]$ and the $[10\bar{1}]$ directions (Fig. 2). The Cu-O-Cu angle is 146° in the $[10\bar{1}]$ chains and 109° in the $[101]$ chains.

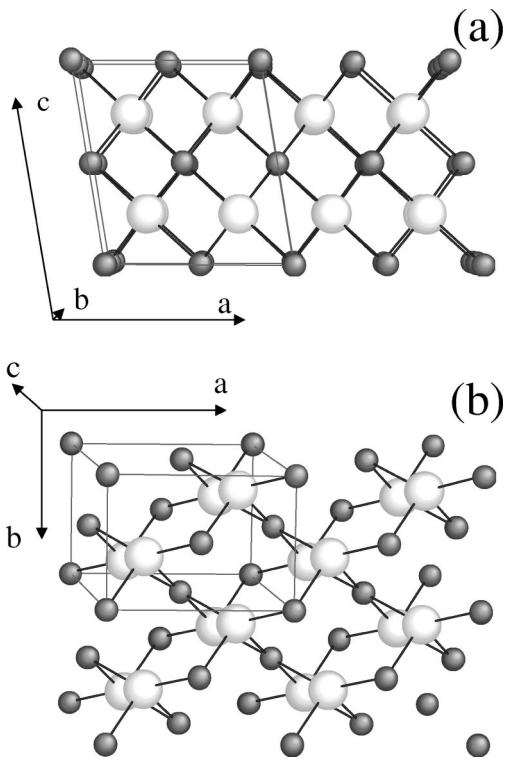


FIG. 1. The crystal structure of CuO (after Asbrink and Norrby). Different projection views of the $2a \times 2b \times c$ cell array are shown: the $ac$-plane view (a) and the $ab$-plane view (b). The unit cell containing four CuO units is indicated by the parallelepiped. The oxygen atoms are light gray; the copper atoms are dark gray.

For the $C_{2h}^6$ space group the factor-group (FG) analysis[12] gives the following set of the zone-center lattice modes: $\Gamma = A_g + 2B_g + 4A_u + 5B_u$. Out of these, three modes $(A_g + 2B_g)$ are Raman active, six modes $(3A_u + 3B_u)$ are IR active, and three modes $(A_u + 2B_u)$ are translational. The $A_u$ modes are polarized along the $b$ axis. The dipole moments of the $B_u$ modes lie within the $ac$ plane, but due to the low symmetry their directions are not exactly determined by the crystal structure.

More recently Åsbrink and Waskowska[17] have refined the CuO structure at 196 K and 300 K using the so called ''less significant reflections'' in the x-ray data analysis and found that less symmetric space group $C_s^4$ $(Cc)$ is also consistent

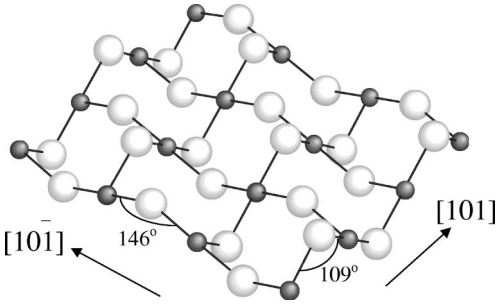


FIG. 2. The Cu-O chains running along the [101] and the [10$\bar{1}$] directions. The oxygen and copper atoms are light gray and dark gray correspondingly. The Cu atoms with the same *b* coordinates only are shown.

with the x-ray diffraction data for both phases. They suggested that the $C_{2h}^6$ space group might result from the time averaging or site averaging of nonequivalent (due to valence fluctuations) atom positions of lower symmetry. Some lattice distortions, especially changes of the Cu-O distances, were clearly detected when passing from RT to 196 K. In general, one can state, that the $C_{2h}^6$ space group is a good approximation to the real structure of the cupric oxide, but some minor deviations from this do not contradict to the x-ray data.

## III. EXPERIMENTAL

### A. Sample preparation and characterization

Single crystals of CuO were obtained from a CuO-PbO-$Bi_2O_3$ melt. The details are described elsewhere.[18] After cooling down the crucible contained randomly oriented large single-crystal pieces of CuO along with inclusions of other phases. From this conglomerate the largest CuO single crystals were extracted and oriented using the x-ray diffraction. As usual, natural crystal faces were presumably of (110) and (1$\bar{1}$0) orientation. This face orientation was used in previous papers where infrared reflectivity measurements were performed. However, for the reasons mentioned above we aimed to obtain the (001) (the *ab* plane) and the (010) (the *ac* plane) crystal faces with a large enough area. These two mutually perpendicular faces were cut on one selected single-crystal sample, which was used for measurement of all the reflectivity spectra presented in this paper. Cuts were polished with a fine 0.06 $\mu$m $Al_2O_3$ powder. Microscopic analysis of the surface[18] has shown that the crystal is twinned. Fortunately, one twin orientation was almost completely dominating; the domains of the alternative twin orientation form narrow stripes covering less than 5% of surface area. Such domination was also confirmed by the x-ray Laue snapshots, where no detectable reflections corresponding to the alternative twin orientation were observed. The structure of twins is such[19] that the *b* axis direction is the same for different twin orientations; all twin reflections are within the *ac* plane. So a minor (less than 5%) contribution of other twin domains is possible for the (010) face reflectivity spectra. For the case of reflection from the (001) face, when $E \| b$, all twins contribute in the same way and twinning has no effect. The Lauegram has shown that (001) and (010) crystal faces were cut with accuracy of 1.8° and 2.1°, respectively. The electron Auger microscopy has shown the presence of only copper and oxygen atoms on the both crystal faces. The area of the (001) face suitable for quantitative optical measurements (i.e., containing no impurity inclusions, having the lowest fraction of the alternative twin orientation), was $\sim 3$ mm$^2$; that of the (010) face was $\sim 4$ mm$^2$.

### B. Reflectance measurement

Infrared near-normal reflectivity spectra were measured from 70 to 6000 cm$^{-1}$ using a Bruker IFS 113*v* FT-IR spectrometer. The average angle of incidence was about 11°. A set of different light sources, beamsplitters, polarizers, and detectors were used to cover this frequency range. The mid-infrared (MIR) spectra from 400 to 6000 cm$^{-1}$ were measured using a globar source, KBr beamsplitter, KRS-5 polarizer, and DTGS and MCT detectors. The far-infrared (FIR) region 70–700 cm$^{-1}$ was studied with the aid of the Hg lamp, a set of mylar beamsplitters, a polyethylene polarizer and the helium-cooled Si bolometer.

The polarizer was mounted in the optical path of the incident beam; no additional polarizers (analyzers) were put in between sample and detector. The transmission properties of the polarizers were measured independently and, when necessary, special care of the correction for the unwanted polarization leakage was taken. Polarizer rotation was performed using a computer-controlled mechanical device.

For the case of reflection from the monoclinic *ac* plane a special three-polarization measurement technique[20] was used. It involves the measurement of three reflectivity spectra per crystal face for different polarizations of almost normally incident light: vertical (0°), horizontal (90°), and diagonal (45°). In principle, the knowledge of these spectra should be enough to calculate the reflectivity for any other polarization direction. In particular, the relation $R(0°)+R(90°)=R(45°)+R(-45°)$ should work. We especially checked the validity of this relation and experimentally proved that it holds with a good accuracy. Such a technique is necessary for monoclinic crystals, where directions of principal dielectric axes depend on frequency.

The sample was mounted with a good thermal contact in a continuous-flow Oxford Instruments cryostat with an automatic temperature control. Spectra were measured at temperatures 300, 250, 240, 230, 220, 210, 200, 180, 150, 100, and 7 K, so that special attention has been paid to the range in the vicinity of $T_{N_1}=230$ K and $T_{N_2}=213$ K. The temperature setting accuracy was about 1 K.

A reference for the absolute reflectivity was provided by *in situ* evaporation of a gold layer on the surface and consecutive repetition of the same set of measurements for every temperature. Such a procedure has compensated errors associated with not only nonideality of the sample face but also the thermal deformation of the cryostat cold finger. To account for a possible drift of a single-beam intensity due to source and detector instability, every sample-channel measurement was accompanied by a measurement of the inten-

sity of the light beam passed via the second (reference) channel without reflection from the sample. The mirror position reproducibility after switching from the sample to the reference channel was checked to be good enough.

## IV. SPECTRA TREATMENT

### A. The dispersion analysis

Let us introduce the orthogonal system of coordinates $\{xyz\}$: $x\|a$, $y\|b$, $z\perp a$, $z\perp b$ so that there is a slight inclination ($\sim 9.5°$) between axes $z$ and $c$. Due to the monoclinic symmetry the whole three-dimensional (3D) dielectric tensor $\hat{\epsilon}$ is the composition of two components: the scalar $\epsilon_b=\epsilon_{yy}$ along the $b$ axis and the 2D tensor $\hat{\epsilon}_{ac}=\left(\begin{smallmatrix}\epsilon_{xx}&\epsilon_{xz}\\ \epsilon_{zx}&\epsilon_{zz}\end{smallmatrix}\right)$ within the $ac$ plane ($\epsilon_{xz}=\epsilon_{zx}$ is expected without external magnetic field). The dispersion formulas are:

$$\epsilon_b(\omega)=\epsilon_b^{\infty}+\sum_{i,A_u}\frac{\omega_{\mathrm{p},i}^2}{\omega_{\mathrm{TO},i}^2-\omega^2-\mathrm{i}\gamma_i\omega}, \tag{1}$$

$$\hat{\epsilon}_{ac}(\omega)=\hat{\epsilon}_{ac}^{\infty}+\sum_{i,B_u}\frac{\omega_{\mathrm{p},i}^2}{\omega_{\mathrm{TO},i}^2-\omega^2-\mathrm{i}\gamma_i\omega}\times\begin{pmatrix}\cos^2\theta_i & \cos\theta_i\sin\theta_i\\ \cos\theta_i\sin\theta_i & \sin^2\theta_i\end{pmatrix}, \tag{2}$$

where $\omega_{\mathrm{TO},i}$—the transverse frequency, $\omega_{\mathrm{p},i}$—the plasma frequency, $\gamma_i$ is the linewidth of the $i$th mode, $\theta_i$—the angle between the dipole moment of the $i$th mode and the $x$ axis (for the $B_u$ modes only), $\epsilon_b^{\infty}$ is the high-frequency dielectric constant along the $b$ axis, and $\hat{\epsilon}_{ac}^{\infty}$ is the high-frequency dielectric tensor within the $ac$ plane. The $b$ axis complex reflectivity $r_b$ and the measured reflectance of the (001) plane for $E\|b$ are expressed via the dielectric function:

$$r_b(\omega)=\frac{1-\sqrt{\epsilon_b(\omega)}}{1+\sqrt{\epsilon_b(\omega)}},\quad R_b(\omega)=|r_b(\omega)|^2. \tag{3}$$

The complex reflectivity tensor $\hat{r}_{ac}$ can be expressed via the dielectric tensor $\hat{\epsilon}_{ac}$ by the matrix formula, which is formally analogous to Eq. (3):

$$\hat{r}_{ac}(\omega)=[\hat{1}-\sqrt{\hat{\epsilon}_{ac}(\omega)}]\cdot[\hat{1}+\sqrt{\hat{\epsilon}_{ac}(\omega)}]^{-1}, \tag{4}$$

where $\hat{1}$ is the unity tensor. The matrix square root naturally means, that the matrix is first reduced to the diagonal form by a proper rotation, the square root is then taken from each diagonal element, and finally it is rotated back to the initial coordinate system. The ''-1'' exponent implies calculation of the inverse matrix.

The reflectance of the (010) plane depends on the direction of the incident light polarization $e=E/|E|$:

$$R_{ac}(\omega,\mathbf{e})=|\hat{r}_{ac}(\omega)\mathbf{e}|^2. \tag{5}$$

The reflectances for values 0°, 45°, and 90° of the angle between the electric field vector and the $x$ axis used in the ''three-polarization'' measurement scheme[20] are expressed in terms of the components of $\hat{r}_{ac}$:

$$R_{00}(\omega)=|r_{xx}(\omega)|^2+|r_{xz}(\omega)|^2,$$

$$R_{45}(\omega)=(|r_{xx}(\omega)+r_{xz}(\omega)|^2+|r_{xz}(\omega)+r_{zz}(\omega)|^2)/2,$$

$$R_{90}(\omega)=|r_{xz}(\omega)|^2+|r_{zz}(\omega)|^2. \tag{6}$$

The phonon parameters can be obtained by fitting of the reflectance spectra using the written above formulas. To obtain the $A_u$ modes parameters the $R_b(\omega)$ spectrum is fitted. The characteristics of the $B_u$ modes, including unknown angles $\theta_i$, can be extracted by simultaneous fitting of three spectra $R_{00}(\omega)$, $R_{45}(\omega)$, and $R_{90}(\omega)$ from the (010) plane.

### B. The Kramers-Kronig analysis

For the case $E\|b$ the Kramers-Kronig (KK) analysis can be performed in a usual way because one of the dielectric axes is parallel to this direction. Due to the low crystal symmetry, the directions of the two other principal dielectric axes in the $ac$ plane depend on the frequency, which precludes the straightforward application of the KK method to the $ac$ plane reflectance data. For this case we used a modified version of this technique, which allows to determine frequency dependence of all the components of the complex reflectivity tensor $\hat{r}_{ac}$, provided that three reflectance spectra $R_{00}(\omega)$, $R_{45}(\omega)$ and $R_{90}(\omega)$ are measured in wide enough frequency range. The details of this KK method generalization are described elsewhere.[21]

For a correct implementation of the KK integration, the reflectivity in the range 6000–37 000 $\mathrm{cm}^{-1}$ was measured using the Woollam (VASE) ellipsometer system at room temperature. At higher frequencies the $\omega^{-4}$ asymptotics was assumed. At low frequencies the reflectivity was extrapolated to a constant. One should mention, that after that procedure some uniform physically unreasonable shift of the complex reflectivity phase was present for the low-temperature data (especially at 7 and 100 K), which is presumably due to neglecting of the temperature dependence of the high-frequency reflectivity. Some correction for that was provided by shifting of the complex reflectivity phase equally at all frequencies in order to make it as close to $\pi$ as possible in several selected frequency points where no strong absorption is observed.

## V. RESULTS AND ANALYSIS

### A. $E\|b$

The reflectance spectra for the (001) plane, when $E\|b$, are shown at Fig. 3. In this configuration only the $A_u$ TO modes should be active. Exactly three strong modes are observed: $A_u^1$ ($\sim 160$ $\mathrm{cm}^{-1}$), $A_u^2$ ($\sim 320$ $\mathrm{cm}^{-1}$), and $A_u^3$ ($\sim 400$ $\mathrm{cm}^{-1}$), which confirms the FG-analysis predictions for the established CuO crystal structure. The most drastic temperature changes take place in the range 350–550 $\mathrm{cm}^{-1}$, where the Reststrahlen band corresponding to very intense lattice mode $A_u^3$ is situated. The reflectivity maximum el-

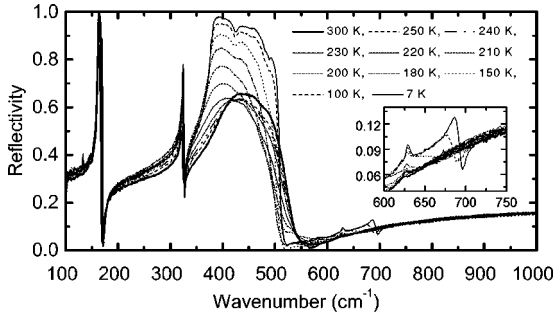


FIG. 3. Reflectance spectra for the (001) plane for polarization $E\|b$ as a function of temperature.

evates from 65 to almost 100%; it moves to lower frequencies upon cooling down the sample. This indicates, that the mode experiences strong softening and narrowing as a temperature is decreased. A sharp feature at $\approx 130\ \mathrm{cm}^{-1}$ is of apparatus origin and should be ignored.

In addition to three strong modes, at least five ''extra'' structures in these reflectivity spectra are detectable ''by eye'' (Fig. 3). The first structure is a dip at $\sim 425\ \mathrm{cm}^{-1}$ just on the top of the Reststrahlen band, which becomes visually evident below 210 K. The second is a $\sim 485\ \mathrm{cm}^{-1}$ structure also on the top of the same Reststrahlen band seen at 100 and 7 K. The third feature is a $\sim 630\ \mathrm{cm}^{-1}$ peak (see inset), which is very small (but observable) at 300 K, and becomes significant at low temperatures. The fourth structure is high-frequency mode $\sim 690\ \mathrm{cm}^{-1}$ (see inset), which is very obvious at 7 K ($690\ \mathrm{cm}^{-1}$) and 100 K ($680\ \mathrm{cm}^{-1}$), still detectable at 150 K ($\sim 650\ \mathrm{cm}^{-1}$), and not seen at higher temperatures, probably, because of strong broadening. The fifth structure is seen at 165–170 $\mathrm{cm}^{-1}$ at the top of the Reststrahlen band of the $A_u^1$ mode (Fig. 4). It is better observable at low temperatures; but even at room temperature the form of the Reststrahlen band differs from a single-mode shape.

The observations ''by eye'' should be accompanied by numerical analysis. The dispersion analysis of spectra has been performed in two stages. In the first stage, in order to determine the characteristics of the principal modes, we have fitted the reflectivity curves with introduction of three modes only. The experimental and fitting curves are compared at Fig. 5(a) for the $T=100$ K. The fit quality is good enough;

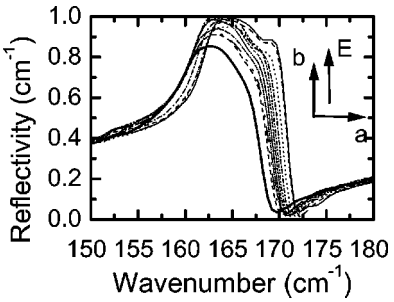


FIG. 4. Reflectance spectra for the (001) plane for polarization $E\|b$ as a function of temperature (enlarged view of the $A_u^1$ mode region).

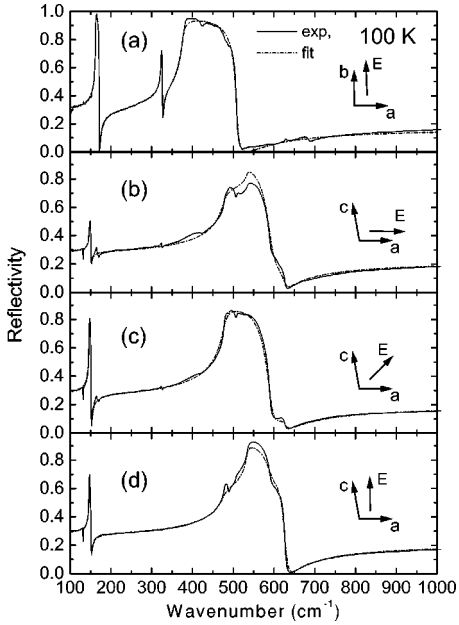


FIG. 5. Fitting of the measured spectra for different polarizations at 100 K by the dispersion formulas.

the deviations are observed only in the range of additional modes. The relative weakness of additional structures ensures that errors associated with the fundamental modes will be small. The parameters of three-principal $A_u$ phonon modes obtained by such a fitting as a function of temperature are shown at Fig. 6. Parameter values at 300 and 7 K are presented in Table I. The LO frequencies $\omega_{\mathrm{LO}}$ were calculated using the $\omega_{\mathrm{TO}}$ and $\omega_{\mathrm{p}}$.

From Fig. 6 a conclusion can be drawn immediately that the $A_u^1$ and $A_u^2$ modes behave in a quite similar way, while

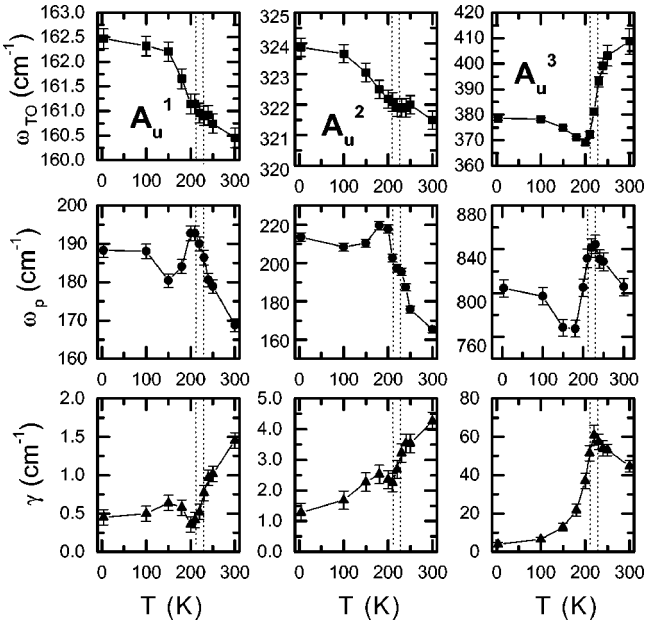


FIG. 6. Parameters of the principal $A_u$ TO modes, obtained by the 3-mode dispersion analysis of the reflectance spectra for the (001) plane, $E\|b$. Vertical dotted lines denote $T_{N1}$ and $T_{N2}$.

TABLE I. Parameters of principal IR-active phonon modes at 300 and 7 K, derived from the dispersion analysis of reflectance spectra. All values are given in $cm^{-1}$, except for the angles $\theta$, which are expressed in degrees. The high-frequency dielectric tensor components are almost temperature independent. Their values at 300 K are $\epsilon_{xx}^{\infty}=7.3$, $\epsilon_{yy}^{\infty}=5.9$, $\epsilon_{zz}^{\infty}=6.8$, $\epsilon_{xz}^{\infty}=-0.8$.

| | 300 K | | | | | 7 K | | | | |
|---|---|---|---|---|---|---|---|---|---|---|
| Mode | $\omega_{TO}$ | $\omega_{LO}$ | $\omega_p$ | $\theta$ | $\gamma$ | $\omega_{TO}$ | $\omega_{LO}$ | $\omega_p$ | $\theta$ | $\gamma$ |
| $A_u^1$ | 160.5 | 168.3 | 166.7 | - | 1.5 | 162.5 | 171.1 | 188.3 | - | 0.5 |
| $A_u^2$ | 321.5 | 324.2 | 169.5 | - | 4.3 | 323.9 | 326.8 | 213.5 | - | 1.3 |
| $A_u^3$ | 408.7 | 535.6 | 805.7 | - | 44.6 | 378.5 | 509.4 | 804.4 | - | 3.8 |
| $B_u^1$ | 144.9 | 149.6 | 123.0 | 53.0° | 1.3 | 146.6 | 151.2 | 121.1 | 54.1° | 1.2 |
| $B_u^2$ | 469.6 | 620.7 | 908.0 | 30.5° | 10.6 | 480.6 | 625.5 | 883.8 | 35.1° | 18.1 |
| $B_u^3$ | 522.8 | 585.5 | 957.2 | −57.6° | 7.0 | 536.2 | 589.1 | 922.6 | −54.7° | 6.5 |

the highest-frequency $A_u^3$ mode is significantly different. The $A_u^1$ and $A_u^2$ modes are steadily hardening with cooling ($\sim$1%), with some increasing of the slope $\partial\omega_{TO}/\partial T$ below $T_N$. In contrast, the $A_u^3$ mode slightly softens with cooling down to the $T_{N1}$, then undergoes a drastic sharp softening ($\sim$10%) in the vicinity of the transition temperature and then hardens with further cooling from $T_{N2}$ down to the helium temperature. The $A_u^2$ and $A_u^3$ modes are relatively narrow at 300 K and exhibit further narrowing with cooling with some dip at the transition temperature. On the contrary, the $A_u^3$ mode is very broad at 300 K, and broadens more with approaching the $T_N$. Its linewidth has a pronounced maximum in between $T_{N1}$ and $T_{N2}$. In the AFM phase it quickly narrows with cooling down.

In the second stage, in order to determine or, at least, estimate parameters of the mentioned ''extra'' modes, additional fitting of spectra with introduction of both principal and ''extra'' modes has been performed (see Fig. 7). It was possible to fit the structures at 167 $cm^{-1}$, 425 $cm^{-1}$, 485 $cm^{-1}$, and 690 $cm^{-1}$. The 630 $cm^{-1}$ peak cannot be fitted by the usual Lorentzian term; the reason is evidently very strange line shape of this mode, which we are not able to explain now. The first fit was performed at 7 K, when additional structures are mostly sharp. Other spectra were fitted in sequence 100,150, . . . ,300 K. At each step the oscillator parameters, corresponding to the previous temperature served as initial approximation for the least-squares fitting. Parameter confidence limits were always calculated by the ''covariant matrix'' method (see error bars at Fig. 7), which takes into account possible correlation of parameters. In this way it was possible to extend curves of modes 167 $cm^{-1}$, 425 $cm^{-1}$, and 480 $cm^{-1}$ up to room temperature; the 690 $cm^{-1}$ mode was fitted only for $T\leqslant 150$ K because at higher temperatures fitting could not give reasonable values of parameters for this mode. The errors in determination of additional modes are relatively larger than those for the principal ones, which is natural, in view of their small intensity. In general, errors are smaller at lower temperatures.

The temperature dependence of TO frequency of the additional mode 167 $cm^{-1}$ is more or less typical for phonons

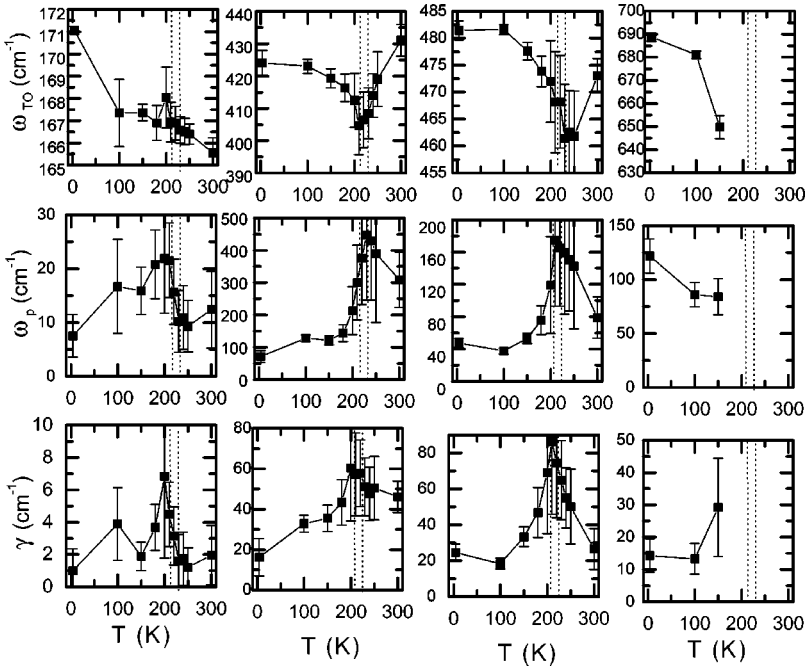


FIG. 7. Parameters of the ''extra'' modes, obtained by the full (both principal and extra modes are considered) dispersion analysis of the reflectance spectra for the (001) plane, $E\|b$. Error bars indicate parameter confidence limits and reflect possible correlation of different parameters. Vertical dotted lines denote $T_{N1}$ and $T_{N2}$.

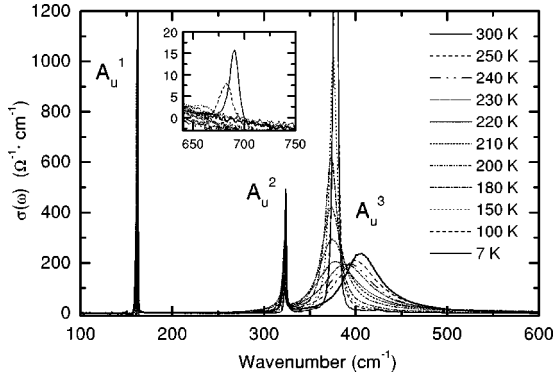


FIG. 8. Optical conductivity obtained by the Kramers-Kronig transformation of reflectance spectra for the (001) plane, $E\|b$ as a function of temperature. Only TO $A_u$ modes should be seen in this configuration. Inset: the ''extra'' mode $\sim 690$ cm$^{-1}$.

(the value of 171 cm$^{-1}$ at 7 K is an artifact of the dispersion analysis with no physical meaning). On the contrary, the 425 and 485 cm$^{-1}$ modes demonstrate a puzzling temperature dependence, similar to that of the $A_u^3$ mode 400 cm$^{-1}$. First of all, there is no indication of disappearance of these modes above the AFM transition, although they are not clearly seen ''by eye.'' Nevertheless, the transition strongly affects parameter values of these modes. Both modes soften strongly above $T_N$ and harden strongly below $T_N$. The modes narrow below $T_N$ (which facilitates their visual observation), and are very broad at higher temperatures with a strong maximum at the transition point. The temperature dependencies of these modes parameters are masked by large error bars, therefore only qualitative conclusions can be drawn. It can be explained by some correlation between parameters of these modes with ones of the $A_u^3$ mode. It is a typical problem for several broad closely located modes. Therefore, it is unreasonable to attribute physical meaning to increasing of the plasma frequency of these modes above 200 K: their plasma frequencies are just subtracted from the plasma frequency of the $A_u^3$ mode without significant influence on the fit quality, which is manifestation of the oscillator strength sum rule. For the 690 cm$^{-1}$ mode the dispersion analysis results confirm visual observations: anomalously strong hardening upon cooling and strong broadening with heating. The latter, probably, precludes satisfactory fitting of this mode at higher temperatures.

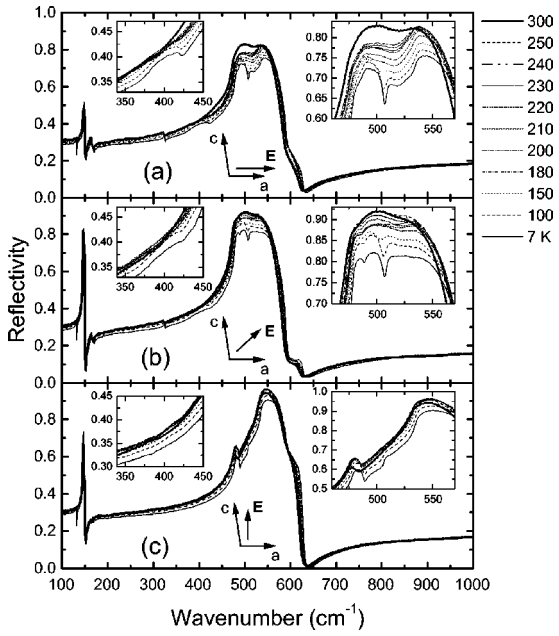


FIG. 9. Reflectance spectra for the (010) plane for different polarizations as a function of temperature. (a) $R_{00}$; (b) $R_{45}$; (c)$R_{90}$.

The curves of the $b$-axis optical conductivity $\sigma_b(\omega) = \omega\, Im\, \epsilon_b(\omega)/4\pi$, obtained by the KK transform of the reflectivity spectra for each temperature, are shown at Fig. 8 (the conductivity is expressed in the practical units $\Omega^{-1}$ cm$^{-1}$). The conductivity is very illustrative to show a remarkable difference between the $A_u^1$ and $A_u^2$ narrow modes and the $A_u^3$ mode exhibiting a puzzling temperature dependence. The sharpness of the $A_u^1$ and $A_u^2$ modes and the absence of the $B_u$ modes contribution to this spectrum confirms a good sample quality and its proper orientation.

### B. $E\|ac$

The reflectance spectra from the (010) plane for three polarizations of the incident light ($R_{00}$, $R_{45}$, and $R_{90}$) are shown at Fig. 9. The $B_u$ TO modes are expected to appear in these spectra.

The narrow mode $B_u^1$ ($\sim 145$ cm$^{-1}$) is clearly observed in all polarizations. Its intensity depends, of course, on the light polarization, i.e., the angle between the electric field vector and the mode dipole moment. A strong Reststrahlen band is seen in the 450–600 cm$^{-1}$ range. The shape and the center position of the band is polarization dependent, which is consistent with a suggestion that it is actually formed by at least two high-frequency intense modes. In the $R_{00}$ ($E\|a$) and $R_{45}$ spectra one can observe some minor contribution from the $A_u^1$ (162 cm$^{-1}$) and $A_u^2$ (324 cm$^{-1}$) modes, which should be, in principle, not observed in this geometry. The possible reason is some misorientation of the sample, therefore projections of the dipole moments of the $A_u$ modes are nonzero, although quite small. In this case these modes should be not in the TO regime, but more close to the LO state, because their dipole moments are almost parallel to the wave vector. As has been already mentioned, a spike at about 130 cm$^{-1}$ is of apparatus origin.

As is in the case of $E\|b$, some extra structures are seen. The first is a broad band in the range 380–425 cm$^{-1}$. It is especially pronounced for $E\|a$, less evident for intermediate polarization and absent for $E\perp a$ (see the left insets in Fig. 9). A dip at 425 cm$^{-1}$, undoubtedly correlates with the dip at the same frequency at reflectance for $E\|b$. The second is a pronounced structure consisting of a peak at $\sim 480$ cm$^{-1}$ and a dip at $\sim 485$ cm$^{-1}$ in the $R_{90}$ spectrum, existing at all temperatures. In spite of proximity of this frequency to additional structure at Fig. 3, a completely different temperature dependence suggests that these modes are separate. The third structure is a dip at $\sim 507$ cm$^{-1}$ on the top of the Reststrahlen band of $R_{00}$ and $R_{45}$ (see the right insets in Fig. 9). This frequency is very close to the LO frequency of the

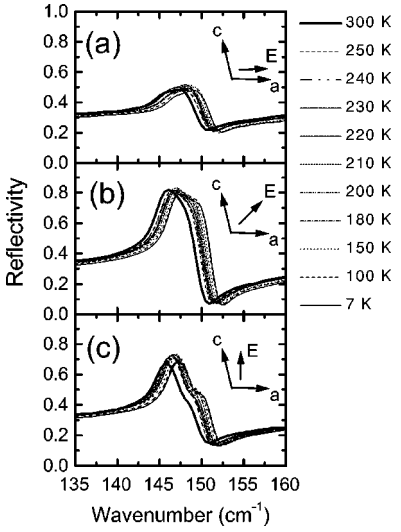


FIG. 10. Reflectance spectra for the (010) plane for different polarizations as a function of temperature (enlarged view of the $B_u^1$ mode region). (a) $R_{00}$; (b) $R_{45}$; (c)$R_{90}$.

$A_u^3$ mode, therefore it is most likely the $A_u^3$ mode almost in the LO regime, which is seen in this spectrum for the same reason as the $A_u^1$ and $A_u^2$ modes are (some misorientation of crystal axes). The fourth structure is seen in the vicinity of the $B_u^1$ mode (Fig. 10). The shape of this mode is such that it is worth to suggest, that it is actually composed of two different modes [see, especially, Fig. 10(c)].

For each temperature a fitting procedure with introduction of 3 oscillators, corresponding to principal $B_u$ modes (one low-frequency and two high-frequency ones) has been performed. The phonon polarization angles were adjusted along with other phonon parameters. Spectra $R_{00}$, $R_{45}$, and $R_{90}$ were fitted at the same time. The fit quality for $T=100$ K is seen in the Figs. 5(b)–5(d). One can see that the $B_u^1$ 145 cm$^{-1}$ mode as well as the general shape of the Reststrahlen band at 450–600 cm$^{-1}$ are satisfactorily reproduced, confirming a suggestion that only three strong phonon modes are present. A bump at about 620 cm$^{-1}$ is fitted without invoking additional Lorentzians: it results from the noncollinearity of the mode and the incident radiation polarizations. Parameter values at 300 and 7 K are presented in Table I.

The temperature dependence of the $B_u$ phonon parameters is presented at Fig. 11. Unlike the case of the $A_u$ modes, there is no significant difference in the temperature dependence of parameters of the low- and high-frequency $B_u$ modes. All modes are monotonically hardening with cooling down, with a positive kink at $T_N$ for the $B_u^3$ mode and a negative kink for the $B_u^2$ mode. The plasma frequencies of all modes have slight maximum at the transition temperature. Two high-frequency modes are much more intense than the $B_u^1$ mode. The linewidth of all the modes doesn't decrease with cooling down. Instead, it increases at low temperatures. One should be careful in a straightforward interpretation of this result, because the line shape is not described perfectly, especially one of the high-frequency modes. The true linewidth is better seen from the optical conductivity graph (see

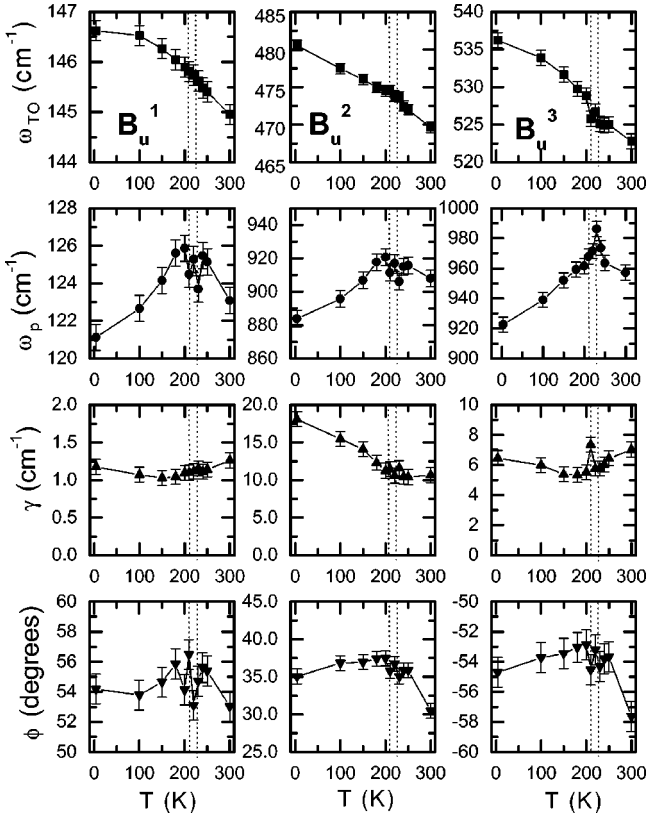


FIG. 11. Parameters of the TO $B_u$ modes, obtained by the 3-mode dispersion analysis of the reflectance spectra for the (010) plane. For each temperature three spectra for different polarizations of the incident light were fitted simultaneously. Vertical dotted lines denote $T_{N1}$ and $T_{N2}$.

below). The oscillator polarization angles do not significantly change with frequency. The maximum angle change is 4°–5°, while the change of the relative angle between different oscillators polarization is less than 2°.

We have tried to fit ''extra'' modes by introduction of additional Lorentian terms to the dielectric function. The attempt was successful only for the structure 147 cm$^{-1}$ near the $B_u^1$ mode. Its characteristics as well as slightly corrected by introduction of additional mode parameters of the $B_u^1$ mode are presented at Fig. 12. A failure of the dispersion model to describe other structures can be explained either by a non-Lorentian shape of ''extra'' modes or by the influence of twinning, which, although less than 5%, could be significant for analysis of weak modes.

To investigate the true shape of the principal phonon modes and additional structures, the KK analysis of the $ac$-plane data for the mentioned set of temperatures was implemented in the extended form.[21] It Fig. 13 all the components of the optical conductivity tensor $\hat{\sigma}_{ac}(\omega) = \omega\, Im\, \hat{\epsilon}_{ac}(\omega)/4\pi$ are plotted for selected temperatures. Note that the off-diagonal component $\sigma_{xz}$ may have any sign unlike the diagonal components $\sigma_{xx}$ and $\sigma_{zz}$ which must be positive.

The polarization angle of the $B_u^2$ mode is 35°, which is close to the direction of the [101] chains. The $B_u^3$ mode is

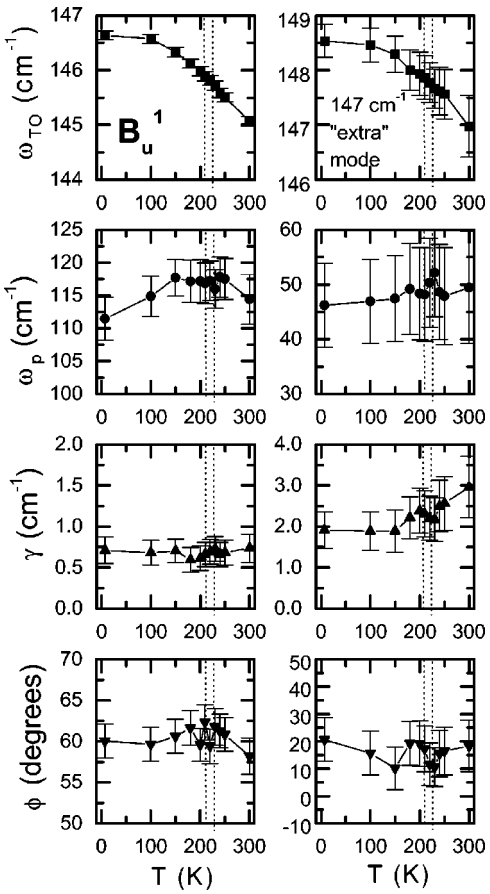


FIG. 12. Parameters of the 147 $cm^{-1}$ ''extra'' mode, and corrected parameters of the $B_u^1$ mode obtained by dispersion analysis of the reflectance spectra for the (010) plane. Error bars indicate parameter confidence limits. Vertical dotted lines denote $T_{N1}$ and $T_{N2}$.

almost orthogonal to the $B_u^2$ mode: the angle is $-55°$, which is close to the $[10\bar{1}]$ chains direction. Therefore, with some approximation one can state, that the $B_u^2$ and $B_u^3$ modes are stretches of the [101] and $[10\bar{1}]$ chains correspondingly, which is in agreement with several lattice dynamical calculations.[10–12,22,23] Note, that such orthogonality is not determined by the crystal symmetry. The polarization angles of both modes are almost temperature independent. The right angle between the dipole moments allows one to switch to the coordinate system formed by them and thus approximately separate the contribution of these modes in the conductivity curves. Figure 14 presents such a conductivities corresponding to these two directions. It is seen that modes are separated indeed, which can be considered as an the additional proof of their orthogonality. It should be stressed that in such a way the conductivity tensor is approximately diagonalized in the range of the modes $B_u^2$ and $B_u^3$ only; for other frequencies, e.g., in the range of the $B_u^1$ mode it is not valid.

## VI. DISCUSSION

### A. Comparison with previous results

A comparison of our data with previously reported results of IR studies of CuO cannot be direct, because we measured

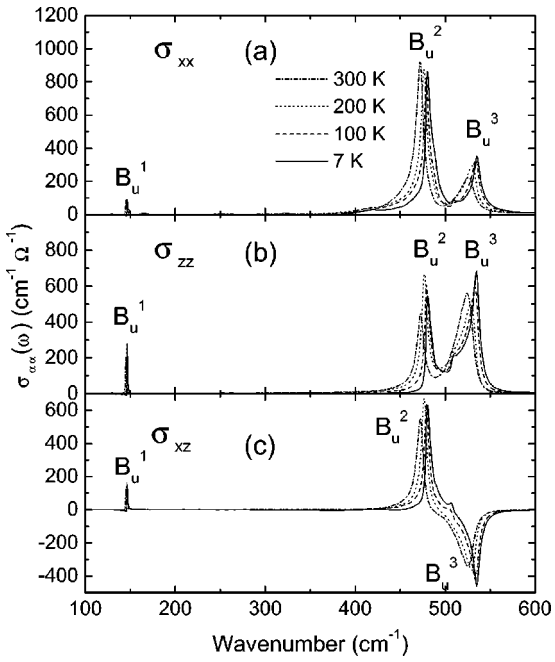


FIG. 13. Components of the optical conductivity tensor $\hat{\sigma}_{ac}(\omega)$ for selected temperatures: (a) $\sigma_{xx}$, (b) $\sigma_{zz}$, and (c) $\sigma_{xz}$.

spectra, where the $A_u$ and $B_u$ modes are separated and excited in purely transverse regime. All the quantitative and even qualitative deviations with previous data (see below) can be ascribed to a different way of spectra measurement and analysis.

In Table II the phonon frequencies at room temperature previously obtained by means of infrared spectroscopy[10–13] as well as neutron scattering[22] are collected. It is seen that the most serious discrepancy between reported values of phonon frequencies takes place for modes $A_u^3$, $B_u^2$, and $B_u^3$, which are very intense and manifest the largest LO-TO frequency splitting. The pure TO mode should have the lowest

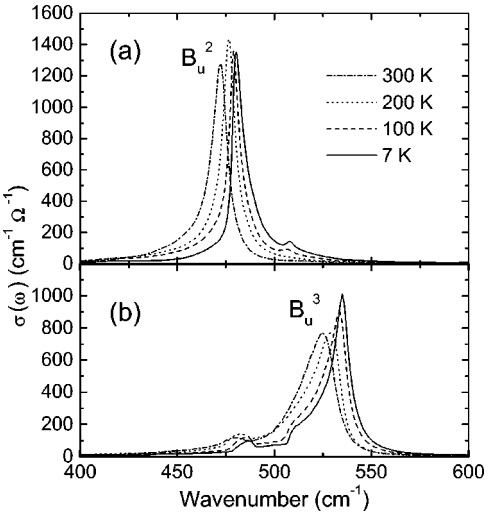


FIG. 14. The diagonal components of the optical conductivity tensor in the coordinate system based on the dipole moments of the $B_u^2$ (a) and $B_u^3$ (b) modes.

TABLE II. Frequencies of the principal $A_u$ and $B_u$ modes (in $cm^{-1}$) at 300 K obtained by different research groups.

| Mode | Kliche *et al.* (Ref. 10) | Guha *et al.* (Ref. 11) | Narang[a] *et al.* (Ref. 12) | Homes *et al.* (Ref. 13) | Reichardt[b] *et al.* (Ref. 22) | This work |
|---|---|---|---|---|---|---|
| $A_u^1$ | 161 | 168 | 163 | 166.5 | 160 | 160.5 |
| $A_u^2$ | 321 | 325 | 324 | 323.7 | 326 | 321.5 |
| $A_u^3$ | 478 | 465 | 444 | 450.0 | 423 | 408.7 |
| $B_u^1$ | 147 | 150 | 147 | 147.6 | 142 | 144.9 |
| $B_u^2$ | 530 | 510 | 515 | 516.0 | 480 | 469.6 |
| $B_u^3$ | 590 | 570 | 586 | 566.0 | 520 | 522.8 |

[a]Data for the 77 K.
[b]Neutron data.

possible frequency, which is in nice agreement with the current result: our reported frequencies are smaller than those reported in other IR spectroscopy papers. One should mention a much better agreement between our data and the results of neutron-scattering experiments,[22] where characteristics of pure TO modes were determined as well.

The softening of the $A_u^3$ mode was reported by Homes *et al.*,[13] who observed a sudden drop of the phonon frequency at the Néel transition from 450 to 430 $cm^{-1}$, i.e., $\sim 5\%$. Our data qualitatively confirm this interesting result. We observe even stronger effect: the TO frequency drops from 410 to 370 $cm^{-1}$ ($\sim 10\%$), which is twice as large as was reported (Fig. 6).

A work by Homes *et al.*,[13] was thus far the only paper, to our knowledge, where IR spectra of single-crystal CuO at low temperatures were studied. Authors didn't report any new IR-active modes below the Néel temperature; it was implied, that no additional lines are present at higher temperatures either. However, an absence of extra IR-active modes is quite strange, if one compares it with an observation of at least five ''unexpected'' lines in the Raman spectra.[15] Conversely, according to our data, several ''extra'' modes are present in IR spectra in the whole 7–300 K frequency range. We believe, that better orientation of the wave vector and polarization of the incident radiation may facilitate observation and analysis of minor IR-active modes.

### B. The $A_u^3$ mode anomaly

The $A_u^3$ mode among other principal IR-active modes behaves in the most anomalous way. It is demonstrated at Fig. 15, where relative RT-normalized TO frequencies and relative linewidths of all six principal modes are plotted together on the same graph. A close relation between magnetic ordering transition at 213–230 K and temperature transformations of this mode is without any doubt.

At 300 K and, especially, at the transition temperature the mode is anomalously broad (12–15 %), which indicates, that it is strongly coupled to some system of quasiparticles. The most probable candidates are the low-energy magnetic excitations. It may be proposed that if there is a strong coupling between spin excitations and the $A_u^3$ lattice mode, the temperature transformations of the mode can be explained by reconstruction of the magnon spectrum upon cooling down below the Néel temperature. It is well established,[3,4,6] that spin correlations in the AFM $[10\bar{1}]$ chains are present well above the Néel temperature. At high temperatures one can consider the magnetic interaction to be of quasi-1D character. In the 1D Heisenberg AFM chains with $S=1/2$ and exchange $J$ there is a continuum of triplet excitations with lower and upper boundary curves[24,25] $\epsilon_{\min}(q)=(\pi J/2)\sin(q)$ and $\epsilon_{\max}(q)=\pi J \sin(q/2)$. A large linewidth of the $A_u^3$ mode can be explained by its interaction with continuum of magnetic excitations. Below the Néel point an exchange interaction in another direction gives rise to long-range magnetic ordering and a continuum of spin excitations collapses to the magnon dispersion curves, which, in turn, results in narrowing of the phonon mode.

The reason for an exceptionally strong interaction of the $A_u^3$ mode with spin excitations one should look for in analysis of its eigenvector. Several lattice dynamical calculations were performed[10–12,22,23] which yielded the lattice mode eigenvectors. According to results of all the calculations this mode is characterized by the largest displacement of the oxy-

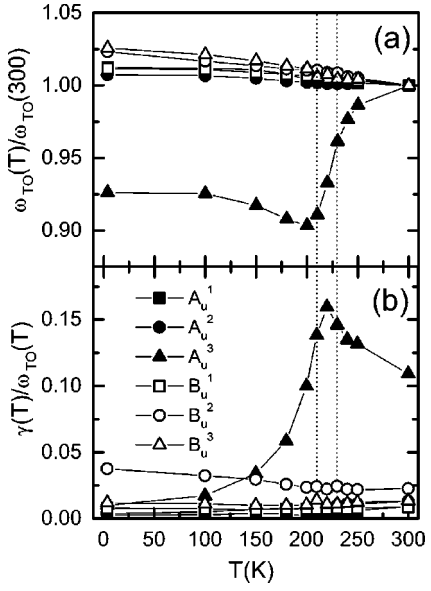


FIG. 15. Relative characteristics of the principal IR-active phonon modes in CuO. (a) The RT-normalized frequency; (b) the relative linewidth. Vertical dotted lines denote $T_{N1}$ and $T_{N2}$.

gen atoms along the *b* axis. It results also in a large dipole moment of this mode. As a consequence, the Cu-O-Cu chain angle experiences the largest variation, when the $A_u^3$ mode is excited. The copper spins are coupled via the superexchange interaction, which is very sensitive to the Cu-O-Cu angle. In the $[10\bar{1}]$ chains the angle is equal to 146° (Fig. 2), which is close to the 180° superexchange. It gives a negative exchange constant and AFM interaction. However, the 90° superexchange is expected to be positive[26] (an indirect confirmation is the ferromagnetic exchange along the [101] chain with angle equal to 109°), and there exists some intermediate angle, where the superexchange is changing sign. Therefore, the motion of atoms, corresponding to excitation of the $A_u^3$ mode can significantly vary the value of the superexchange coupling constant. A strong chain bending probably could alternate the exchange sign.

Due to energy and momentum conservation a zone-center phonon can couple to a pair of magnons (bimagnon) having opposite wave-vectors and one-half frequency of the phonon. Another option is interaction with a single zone-center optical magnon of the same energy. The magnon dispersion curves have been studied by inelastic neutron scattering.[3,6] One acoustic and one optical branch were observed; the energy of optical magnon at the $\Gamma$ point is 5.6 THz (187 $cm^{-1}$), which is very close to one-half of the $A_u^3$ mode frequency (370–380 $cm^{-1}$ at low temperatures), while no optical magnons near 370–410 $cm^{-1}$ were observed. Therefore, taking into account the energy conservation considerations the ''bimagnon'' or, in particular ''optical bimagnon'' scenario of resonant phonon-magnon coupling is the most probable. The parity-based selection rules for the mentioned processes are rather nontrivial in a such a low-symmetry system as CuO, therefore their discussion is a subject of the further publications. A more detailed theory of this effect has to be developed.

### C. Other signatures of spin-phonon interaction

The anomalous properties of the $A_u^3$ mode is not the only manifestation of the spin-phonon interaction in CuO (although the most prominent one). Other modes also demonstrate some anomalies, most likely related to the magnetic ordering.

One type of anomaly is unusually strong hardening of some ''extra'' modes below $T_N$. The most outstanding example is reported in this work hardening of the 690 $cm^{-1}$ mode from 650 $cm^{-1}$ at 150 K to 690 $cm^{-1}$ at 7 K and strong hardening of the the Raman-active 240 $cm^{-1}$ mode found by Chen *et al.*[15] To our mind, these effects are related. We would follow the idea of explanation given by the same authors. The phenomenon can be viewed as a nonresonant spin-phonon interaction, when spin products in the Heisenberg Hamiltonian can be approximated by their effective averages. In this case the temperature dependence of the phonon frequency is expressed by:

$$\omega_n^2(T) = \omega_{n0}^2 + \sum_{ij} C_{ij}^n \cdot \langle S_i S_j \rangle (T). \tag{7}$$

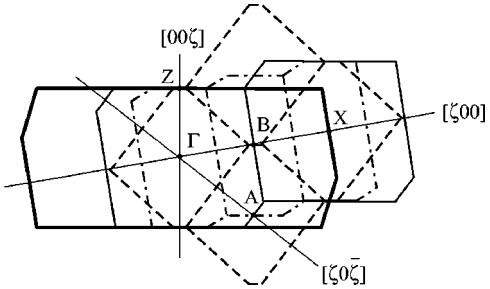


FIG. 16. The *ac*-plane projection of the Brillouin zones corresponding to different unit cells. Thick solid line—primitive cell $\{a,(a+b)/2,c\}$, solid line—unit cell $\{a,b,c\}$, dashed line—$\{a+c,b,a-c\}$, dashed-dotted line $\{2a,b,c\}$.

The $C_{ij}^n$ coefficients are characteristics of spin-phonon interaction; in principle, they may have any sign, depending on the eigenvector of the particular phonon mode. The mode strong hardening is supposedly due to the second ''spin'' term: magnetic ordering gives additional lattice rigidity.

The same phenomenon is possibly responsible for another anomaly, namely, the change of slope $\partial\omega_{TO}/\partial T$ of the principal phonon modes at the Néel point (see Figs. 6 and 11). It is seen that for the modes $A_u^1$, $A_u^2$, and $B_u^3$ the slope is higher in the AFM phase, while for the $B_u^2$ mode the slope is higher at $T > T_N$; for the $B_u^1$ mode it does not change at all. Such a difference can be explained by different values and signs of coefficients $C_{ij}^n$.

### D. ''Extra'' zone-center modes and zone folding

Activation of additional phonon modes in infrared and Raman spectra is usually a signature of unit cell multiplication and zone folding. Such activation is in effect in CuO. As is stated above, several ''extra'' IR-active modes are observed. In the Raman spectra five new modes were detected at low temperatures.[15] Authors related their frequencies to the phonon dispersion curves obtained by inelastic neutron scattering[22] at the zone boundary point. In the paper of Chen *et al.*[15] this point was referred to as $Z'$. We follow the original notation and designate it by $X$ (see Fig. 4 in a paper of Reichardt *et al.*[22]).

At Fig. 16 the Brillouin zones corresponding to several schemes of the unit cell multiplication are drawn (a projection to the *ac* plane). In these schemes different symmetry points fold to the zone center. It is easy to prove, that folding of the $X$ point to the zone center is equivalent to disappearance of the nontrivial translation $(a+b)/2$, or base centering of the space group. In this case the primitive cell should increase at least two times.

In Table III ''extra'' IR active and Raman-active mode frequencies are collected. Each mode frequency is related to close phonon energy (if any) in symmetry points $X(1,0,0)$, $A(1/2,0,1/2)$, $B(1/2,0,0)$, or $C(0,1/2,0)$ at 300 K. To make comparison more reliable, the ''extra'' modes frequencies are taken at temperature as close as possible to 300 K. One can see, that many modes (all Raman-active and several IR-active ones) have close analogs at the $X$ point. At the same

TABLE III. Frequencies (in $cm^{-1}$) of zone-center ''extra'' modes, obtained from IR and Raman spectra, and close phonon frequencies (also in $cm^{-1}$) in some off-center symmetry points of the Brillouin zone, obtained by inelastic neutron scattering at 300 K. IR and Raman data (with the exception of the 690 $cm^{-1}$ mode) are presented at temperatures as close as possible to 300 K.

| IR/Raman (Ref. 15) data | | Inelastic neutron-scattering data (Ref. 22) | | | |
|---|---|---|---|---|---|
| | | X | A | B | C |
| Activity | Frequency | (1,0,0) | (0.5,0,0.5) | (0.5,0,0) | (0,0.5,0) |
| IR | 690 | ? | ? | ? | ? |
| IR | 630 | 630 | - | 633 | - |
| Raman | 507 | 513 | - | - | - |
| IR ($E\|b$) | 480 | - | 485 | 473 | 487 |
| IR ($E\|ac$) | 475 | - | 485 | 473 | 487 |
| IR | 430 | 437 | - | - | - |
| Raman | 331 | 330 | - | - | - |
| Raman | 240 | 243 | - | - | - |
| Raman | 218 | 220 | 223 | - | - |
| Raman | 175 | 177 | - | - | - |
| IR | 165 | - | 167 | - | - |
| IR | 147 | - | 143 | - | 150 |

time, other IR-active modes (147, 165, 475, and 480 $cm^{-1}$) could be phonons from the *A* point, or, in some cases, from the *B* or *C* points. The 690 $cm^{-1}$ mode is a special case: due to strong hardening of this mode with cooling and failure to observe it at high temperatures, the comparison to the 300 K dispersion data is impossible. In addition, the mode energy is higher than the upper limit of the reported frequency region in the neutron-scattering experiments (20 THz, or 667 $cm^{-1}$). The phonon dispersion curves at low temperatures in broader energy interval are desirable.

Although some ''extra'' modes have analogs in the *B* or *C* points, folding of the *A* and *X* points to the zone center (the $A+X$ folding scheme) is the simplest option to explain appearance of all ''extra'' modes. It corresponds to the ''diagonal'' doubling of the unit cell $\{a,b,c\}\rightarrow\{a+c,b,a-c\}$ (see Fig. 16). This scenario looks attractive, because crystal axes correspond to principal anisotropy directions for several physical properties (exchange constants, sound velocity, principal dielectric axes, etc.), and the unit cell is the same as the magnetic unit cell in the AFM phase.[2]

In the framework of this scenario the $A_u^3$ principal mode, the 485 $cm^{-1}$ and the 425 $cm^{-1}$ ''extra'' modes should be the phonon modes from the points $\Gamma$, *A*, and *X* correspondingly belonging to the same dispersion branch, according to ''rigid-ion'' modelling of dispersion curves by Reichardt *et al.*[22] It is in a good agreement with some similarity of temperature dependencies of parameters of these modes (see Figs. 6 and 7).

In summary, we propose, that in reality the crystal structure is more complicated, than was considered before; it is the case, to our mind, already at room temperature, because most of ''extra'' IR-active modes are present in the whole temperature range. Based on the fact that IR-active and Raman-active modes have different frequencies one can suggest that the crystal space group is still centro-symmetric, although the copper atoms are not necessarily located in the $C_i$ position. However, the alternative space group for the CuO, proposed by Asbrink and Waskowska, is not centrosymmetric ($C_s^4$); the solution of this mismatch is unclear.

One of the central issues is the mechanism of the unit-cell multiplication and formation of superstructures. There exist a variety of examples of such effect, when ''extra'' IR and/or Raman modes are emerging, which are undoubtedly the zone-boundary folded phonons. In the extensively studied compounds $CuGeO_3$ and $\alpha'$-$NaV_2O_5$ the unit cell doubles as a result of spin-phonon interaction, and IR modes are observed.[27,28] Another example present compounds with a charge disproportionation, out of those the $BaBiO_3$ is probably the most famous one. In this system the bismuth is disproportionated according to scheme: $2\ Bi^{4+}\rightarrow Bi^{3+}+Bi^{5+}$, and atoms in different valence states form superstructure, which is a reason for ''extra'' quite strong IR line.[29]

The Jahn-Teller nature of the $Cu^{2+}$ ions makes one to consider also a collective Jahn-Teller effect as a possible engine of superlattice formation. It is worth mentioning that lattice distortions due to this effect are often observed in perovskite manganese oxides (the Jahn-Teller ion there is $Mn^{3+}$), known for their possession of the colossal magnetoresistance phenomenon.[30] The electron-lattice coupling in these compounds is responsible for a variety of unusual effects like charge, spin, and orbital ordering. Although the copper site in the CuO is less symmetric than one in an ideal perovskite structure, we cannot exclude a further lowering of the symmetry due to Jahn-Teller effect.

So the question about particular type of spin-charge-lattice ordering in CuO is open. It could be closely connected with formation of inhomogeneity phases in cuprates. Undoubtedly, to circumvent this problem more experiments, e.g. the low-temperature structure refinement by the single-crystal neutron diffraction,[31] has to be conducted.

TABLE IV. A comparison of the high-frequency dielectric function and oxygen transverse effective charges for the cupric oxide CuO and some relevant copper oxides.

| Compound | $\epsilon^{\infty}$ | $e_T^*$ (e) |
|---|---|---|
| CuO, $E\|[010]$ | 5.9 | 1.96 |
| CuO, $E\|[101]$ | 6.2 | 2.06 |
| CuO, $E\|[10\bar{1}]$ | 7.8 | 2.12 |
| $Cu_2O$[33] | 6.5 | 1.91 |
| $La_2CuO_4$, $E\perp c$[34] | 6.0 | 2.05 |
| $YBa_2Cu_3O_6$, $E\perp c$[34] | 5.0 | 2.11 |
| $Bi_2SrLaCuO_y$, $E\perp c$[34] | 6.0 | 2.35 |
| $(Ca,Sr)CuO_2$, $E\perp c$[34] | 8.5 | 2.38 |

### E. High-frequency dielectric function

The reflectivity and the dielectric function in the mid-infrared range well above the maximum phonon energy ($\sim$0.08 eV) but below the optical gap ($\sim$1.3 eV) are determined by the electronic polarizability. We observe significant difference between values of mid-infrared reflectivity for different polarizations. It results in an appreciable anisotropy of the high-frequency dielectric tensor. The temperature dependence of the mid-IR reflectivity is small, therefore, we discuss only room-temperature data. All the components of the $\hat{\epsilon}^{\infty}$ can be found from the dispersion analysis of spectra; their values are listed in the caption to the Table I.

The smallest value of $\epsilon^{\infty}$ is observed along the $b$ axis: $\epsilon_b^{\infty}=5.9$; it is apparently one of the principal values of the dielectric tensor. The diagonalization of the tensor gives directions and values of maximal and minimal levels of $\epsilon^{\infty}$ within the $(ac)$ plane. The maximal value $\epsilon_{\max}^{\infty}=7.8$ is observed along the direction, corresponding to the angle $\phi_{\max}=-36°$, the minimal value $\epsilon_{\min}^{\infty}=6.2$ is along the orthogonal direction for $\phi_{\min}=54°$. One can see that direction $\phi_{\max}$ is very close to direction of the $[10\bar{1}]$ chains ($\phi_{[10\bar{1}]}=-42.5°$) while $\phi_{\min}$ almost exactly corresponds to $\phi_{[101]}=52.8°$. In other words, the high-frequency dielectric constant within the $(ac)$ plane is maximal along the $[10\bar{1}]$ direction, and minimal along the [101] direction (see Table IV).

An ellipsometric determination of the high-frequency dielectric function of polycrystalline CuO sample[32] yielded $\epsilon^{\infty}=6.45$, which is in a good agreement with the average quantity $(\epsilon_{xx}^{\infty}+\epsilon_{yy}^{\infty}+\epsilon_{zz}^{\infty})/3=6.6$ obtained here. Homes *et al.*[13] reported somewhat different values of the $\hat{\epsilon}^{\infty}$ components, e.g., $\epsilon_{yy}=6.7$, which is higher than the value 5.9 obtained here. Such deviation can be explained by the mixed LO-TO excitation of polarization waves due to reflection from a different crystal face.

The value of $\epsilon^{\infty}$ is determined by the static ionic copper and oxygen polarizability. From Table IV one can see that the $\epsilon^{\infty}$ in CuO is similar to that in $Cu_2O$ (Ref. 33) and layered undoped cuprates.[34]

### F. Effective charges

Another characteristic derived from the infrared spectra is an effective ionic charge. The cupric oxide contains only two atoms, therefore effective charges of copper and oxygen can be unambiguously calculated using the sum rule and electrical neutrality condition, unlike the case of more complex oxides.[35,36] The most important is the transverse (Born) charge $e_{\mathrm{T}}^*$, which involves both static (ionic) and dynamic (electronic) contributions to the dipole moment, induced by the external electric field. In the case of the anisotropic system like CuO the well-known formulas for $e_{\mathrm{T}}^*$ in the cubic diatomic crystals[34,35] should be slightly modified. The transverse effective charge is anisotropic and depends on the polarization of the probing electric field $E$:

$$e_{\mathrm{T}}^{*2}(E)=\frac{v_c}{4\pi}\frac{\mu}{4}\sum_i \omega_{\mathrm{p},i}^2\cos^2(\widehat{E,m_i}), \tag{8}$$

where $v_c$ is the volume of the unit cell, containing four Cu-O pairs, $\mu$ is the reduced mass of the Cu and O atoms, $\omega_{\mathrm{p},i}$ and $m_i$—the plasma frequency and the dipole moment of the $i$th IR-active phonon mode. The values of $e_{\mathrm{T}}^*$ along the [010] ($b$ axis), the [101] and the $[10\bar{1}]$ directions are largely determined by the strong phonon modes $A_u^3$, $B_u^2$, and $B_u^3$ correspondingly, because their dipole moments are oriented (almost) parallel to these directions. The anisotropy of the transverse effective charge appears to be relatively small; its value is about two electrons (see Table IV).

The Scott charge $Ze$ is related to the transverse charge via the high-frequency dielectric constant $Ze=e_{\mathrm{T}}^*(\epsilon^{\infty})^{-1/2}$. It is thought to be largely associated with a static (ionic) contribution to the dipole moment.[35] Although this formula is derived for cubic binary compounds, it can be applied for estimation of the average value of $Ze$ in CuO, provided that one uses the average transverse charge and the average $\epsilon^{\infty}$ value. Substitution of $e_{\mathrm{T}}^*=2.05e$ and $\epsilon^{\infty}=6.6$ yields the average Scott charge equal to $0.8e$. The value of $Ze$ divided to the nominal valence is often considered as the degree of ionicity;[35] for the CuO it appears to be about 40%.

In the $Cu_2O$ the value of $e_{\mathrm{T}}^*$ for the oxygen atom is about $1.9e$ (Ref. 36) which is slightly smaller than its value in CuO (see Table IV). Although the difference is not large, it is natural to explain it by larger dynamical electronic contribution to the transverse charge in CuO obtained for layered cuprates. An excellent review of effective charges in various layered copper oxides is given in the work of Tajima *et al.*[34] The copper and oxygen effective charges were estimated from the oscillator strength of the stretching mode in the $CuO_2$ plane. The value of $e_{\mathrm{T}}^*$ was found to vary in a broad range from $2.05e$ for $La_2CuO_4$ to $3.00e$ for $Sr_2CuO_2Br_2$. A clear correlation between $e_{\mathrm{T}}^*$ and interatomic Cu–O distance was observed: the increasing of this distance is accompanied by increasing of the effective charge. In Table IV a comparison is given between $e_{\mathrm{T}}^*$ in CuO and one in selected layered cuprates with a value of the Cu–O distance close to that in the CuO (1.95 Å). A good correspondence between the transverse effective charge values points to a possible similarity of the electronic state of copper and oxygen in the cupric oxide and in the $CuO_2$ planes of undoped layered cuprate compounds, especially $La_2CuO_4$ and $YBa_2Cu_3O_6$.

## VII. CONCLUSIONS

We have measured far- and mid-infrared reflectivity spectra of monoclinic CuO from the (010) and (001) crystal faces in wide temperature range. We obtained characteristics of pure TO $A_u$ and $B_u$ modes separately. Our data finally confirm that there are $3A_u+3B_u$ intense modes, in accordance with prediction of the FG analysis for the $C_{2h}^6$ space group.

We report existence of several ''extra'' less intense IR-active modes in CuO. Analysis of the phonon dispersion curves leads to the conclusion that each ''extra'' IR active as well as reported earlier[15] Raman-active mode could be folded phonon from either $X$ (1, 0, 0) or $A$ (1/2, 0, 1/2) symmetry points. Such folding is compatible with the ''diagonal'' doubling of the unit cell with the basis $\{a+c,b,a-c\}$. So the space group in reality is lower than that was considered, but still centro-symmetric.

The 690 $cm^{-1}$ ''extra'' IR-active mode exhibits anomalous hardening, similar to behavior of the 240 $cm^{-1}$ Raman mode; the reason could be in additional rigidity of lattice due to magnetization, a special manifestation of the spin-phonon interaction. Another effect, which can be explained in a similar way, is a slope change of the phonon frequencies vs temperature at the Néel point.

The anomalous softening and narrowing of the $A_u^3$ mode 410 $cm^{-1}$ we explain by its strong resonance coupling to the optical or acoustic bimagnons. Reconstruction of magnetic excitations spectrum at the AFM transition strongly affects the phonon characteristics.

In summary, the CuO demonstrates a variety of anomalous properties, which show complex interplay of spin, charge, and phonon subsystems already in the simplest copper(II) oxide. A further insight into physics of CuO may contribute to elaboration of noncontradictory picture of antiferromagnetism and superconductivity in the high-$T_c$ cuprates.

## ACKNOWLEDGMENTS

This investigation was supported by the Netherlands Foundation for Fundamental Research on Matter (FOM) with financial aid from the Netherlandse Organisatie voor Wetenschappelijk Onderzoek (NWO). The activity of A.B.K., E.A.T., and A.A.B. was also supported by the Russian Foundation for Basic Research (RFBR), Grant No. 99-02-17752. A lot of thanks we address to H. Bron and F. van der Horst (University of Groningen) for invaluable help in samples characterization.

[1] J. Zaanen, G.A. Sawatzky, and J.W. Allen, Phys. Rev. Lett. **55**, 418 (1985).
[2] B.X. Yang, T.R. Thurston, J.M. Tranquada, and G. Shirane, Phys. Rev. B **39**, 4343 (1989).
[3] M. Ain, W. Reichardt, B. Hennion, G. Pepy, and B.M. Wanklyn, Physica C **162-164**, 1279 (1989).
[4] M. O'Keeffe and F.S. Stone, J. Phys. Chem. Solids **23**, 261 (1961).
[5] U. Kobler and T. Chattopadhyay, Z. Phys. B: Condens. Matter **82**, 383 (1991).
[6] T. Chattopadhyay, G.J. McIntyre, C. Vettier, P.J. Brown, and J.B. Forsyth, Physica B **180**, 420 (1992).
[7] Z.V. Popovic, C. Thomsen, M. Cardona, R. Liu, G. Stanisic, R. Kremer, and W. Konig, Solid State Commun. **66**, 965 (1988).
[8] J. Hanuza, J. Klamut, R. Horyn, and B. Jezowska-Trzebiatowska, J. Mol. Struct. **193**, 57 (1989).
[9] L. Degiorgi, E. Kaldis, and P. Wachter, Physica B **153-155**, 657 (1988).
[10] G. Kliche and Z.V. Popovic, Phys. Rev. B **42**, 10 060 (1990).
[11] S. Guha, D. Peebles, and T.J. Wieting, Bull. Mater. Sci. **14**, 539 (1991); S. Guha, D. Peebles, and T.J. Wieting, Phys. Rev. B **43**, 13 092 (1991).
[12] S.N. Narang, V.B. Kartha, and N.D. Patel, Physica C **204**, 8 (1992).
[13] C.C. Homes, M. Ziaei, B.P. Clayman, J.C. Irwin, and J.P. Franck, Phys. Rev. B **51**, 3140 (1995).
[14] M.V. Belousov and V.F. Pavinich, Opt. Spectrosc. **45**, 771 (1978); V.F. Pavinich and M.V. Belousov, *ibid.* **45**, 881 (1978); V.F. Pavinich and V.A. Bochtarev, *ibid.* **65**, 640 (1988);
[15] X.K. Chen, J.C. Irwin, and J.P. Franck, Phys. Rev. B **52**, R13 130 (1995).
[16] S. Asbrink and L.-J. Norrby, Acta Crystallogr., Sect. B: Struct. Crystallogr. Cryst. Chem. **26**, 8 (1970).
[17] S. Asbrink and A. Waskowska, J. Phys.: Condens. Matter **3**, 8173 (1991).
[18] A.A. Bush, V.Ya. Shkuratov, A.B. Kuz'menko, and E.A. Tishchenko (unpublished).
[19] G.N. Kryukova, V.I. Zaikovskii, V.A. Sadykov, S.F. Tikhov, V.V. Popovskii, and N.N. Bulgakov, J. Solid State Chem. **74**, 191 (1988); V.A. Sadykov, S.F. Tikhov, G.N. Kryukova, N.N. Bulgakov, V.V. Popovskii, and V.N. Kolomiichuk, *ibid.* **74**, 200 (1988).
[20] A.B. Kuz'menko, E.A. Tishchenko, and V.G. Orlov, J. Phys.: Condens. Matter **8**, 6199 (1996).
[21] A.B. Kuz'menko, E.A. Tishchenko, and A.S. Krechetov, Opt. Spectrosc. **84**, 402 (1998).
[22] W. Reichardt, F. Gompf, M. Ain, and B.M. Wanklyn, Z. Phys. B: Condens. Matter **81**, 19 (1990).
[23] J.C. Irwin, T. Wei, and J. Franck, J. Phys.: Condens. Matter **3**, 299 (1991).
[24] J. des Cloizeaux and J.J. Pearson, Phys. Rev. **128**, 2131 (1962).
[25] T. Yamada, Progr. Phys. Jpn. **41**, 880 (1969).
[26] J. Goodenough, *Magnetism and Chemical Bond* (John Wiley & Sons, New York, 1963).
[27] A. Damascelli, D. van der Marel, F. Parmigiani, G. Dhalenne, and A. Revcolevschi, Phys. Rev. B **56**, R11 373 (1997).
[28] M.N. Popova, A.B. Sushkov, A.N. Vasil'ev, M. Isobe, and Yu. Ueda, Pis'ma Zh. Éksp. Teor. Fiz. 65, 711 (1997) [JETP Lett. **65**, 743 (1997)].
[29] S. Uchida, S. Tajima, A. Masaki, S. Sugai, K. Kitazawa, and S. Tanaka, J. Phys. Soc. Jpn. **54**, 4395 (1985).
[30] *Colossal Magnetoresistance, Charge Ordering and Related Prop-*

*erties of Manganese Oxides*, edited by C.N.R. Rao and B. Raveau, (World Scientific Publishers, 1998).
[31] D.V. Sheptyakov, V.Yu. Pomjakushin, and G.J. McIntyre, Physica C **321**, 103 (1999).
[32] T. Ito, H. Yamaguchi, T. Masumi, and S. Adachi, J. Phys. Soc. Jpn. **67**, 3304 (1998).
[33] C. Noguet, C. Schwab, C. Sennett, M. Sieskind, and C. Viel, J. Phys. **26**, 317 (1965).
[34] S. Tajima, T. Ido, S. Ishibashi, T. Itoh, H. Eisaki, Y. Mizuo, T. Arima, H. Takagi, and S. Uchida, Phys. Rev. B **43**, 10 496 (1991).
[35] F. Gervais, Solid State Commun. **18**, 191 (1976).
[36] F. Gervais, P. Echegut, J.M. Bassat, and P. Odier, Phys. Rev. B **37**, 9364 (1988).